

Single-molecule force spectroscopy reveals signatures of glassy dynamics in the energy landscape of ubiquitin

JASNA BRUJIĆ^{1*}, RODOLFO I. HERMANS Z.^{1,2}, KIRSTIN A. WALTHER^{1,3} AND JULIO M. FERNANDEZ^{1*}

¹Department of Biological Sciences, Columbia University, New York, New York 10027, USA

²Department of Applied Physics and Applied Mathematics, Columbia University, New York, New York 10027, USA

³Department of Physics, Columbia University, New York, New York 10027, USA

*e-mail: jb2379@columbia.edu; jfernandez@columbia.edu

Published online: 1 April 2006; doi:10.1038/nphys269

The conformational energy landscape of a protein out of equilibrium is poorly understood. We use single-molecule force-clamp spectroscopy to measure the kinetics of unfolding of the protein ubiquitin under a constant force. We discover a surprisingly broad distribution of unfolding rates that follows a power law with no characteristic mean. The structural fluctuations that give rise to this distribution reveal the architecture of the protein's energy landscape. Following models of glassy dynamics, this complex kinetics implies large fluctuations in the energies of the folded protein, characterized by an exponential distribution with a width of $5\text{--}10k_{\text{B}}T$. Our results predict the existence of a 'glass transition' force below which the folded conformations interconvert between local minima on multiple timescales. These techniques offer a new tool to further test statistical energy landscape theories experimentally.

The glassy model of multiple traps in the native protein landscape was first proposed by Frauenfelder on the basis of ligand binding experiments^{1,2}. Thermal motion of the folded protein explores local fluctuations of the secondary structure, the dynamics of which is crucial for the optimal functioning of the protein³. Complex energy landscape models of proteins are often proposed⁴⁻⁷, and the conformational heterogeneity of the native-state ensemble has been characterized experimentally⁸. Recent work relating the structure and dynamics of human ubiquitin has predicted an unprecedented diversity in the conformations of the native-state ensemble⁹, inferred from the structural motion detected by NMR relaxation experiments. However, the most direct demonstration of the ruggedness of the protein energy landscape under equilibrium conditions has been done at the single-molecule level. For example, fluorescence experiments have identified a conformational diversity in the fluctuations of folded protein molecules at room temperature, in the activity of enzymes in biochemical reactions¹⁰⁻¹² and the correlations of fluorescence lifetimes of conformations of the same protein molecule^{13,14}. These experiments suggest dynamic fluctuations on multiple timescales, and measure a power-law distribution of their lifetimes.

In contrast to these observations, under non-equilibrium conditions protein unfolding is claimed to have a smooth energy landscape¹⁵, lacking the features characteristic of glassy systems. In conventional folding (unfolding) experiments, the proteins are driven out of equilibrium by chemical denaturants and large temperature jumps. In these macroscopic measurements, the pathways are averaged out in the ensemble, such that the energy landscape appears smooth with few (if any) stable intermediates under a given set of unfolding conditions.

Single-molecule force spectroscopy can be used to directly examine the energy fluctuations in the unfolding landscape of a protein. As force is present in many biomechanical processes, it is a natural variable for probing the protein free-energy landscape. Proteins are mechanically stable entities due to the

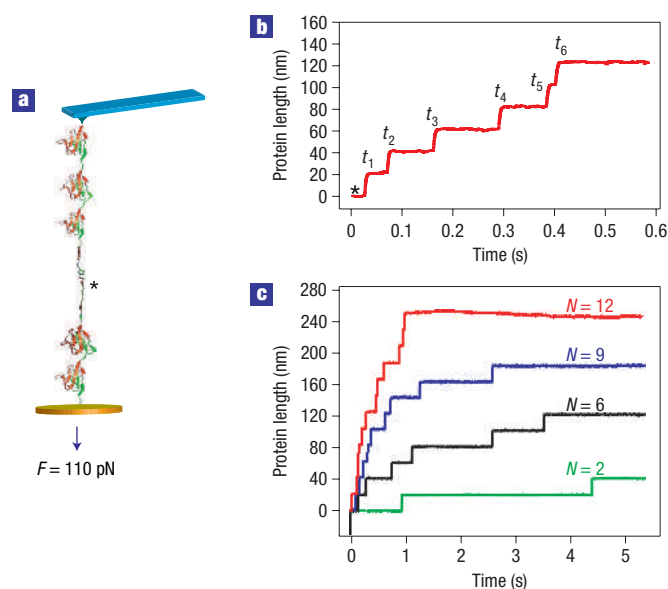


Figure 1 AFM force-clamp spectroscopy experiments on single polyproteins. **a**, A ubiquitin chain of six modules is picked up by the cantilever and held under a constant stretching force of 110 pN. **b**, The individual modules unfold stochastically (see asterisks), as shown by the stepwise increases of length 20 nm in the length versus time measurement. We analyse the dwell times to each unfolding event (from the time of the force application), labelled t_k , to reveal the protein kinetics. (Zero displacement is set at the point where the molecule is taut.) **c**, Ubiquitin chains with a varying number of protein modules, $N \leq 12$, are picked up from the surface resulting in unfolding trajectories of different lengths. Here, N is the same as the number of observed unfolding events, k_{\max} .

network of native contacts that keep the folded structures intact¹⁶. The presence of an external stretching force probes the conformational diversity of the protein out of equilibrium, using the mechanical stability of each conformation as its structural fingerprint¹⁷. The complex and dynamic network of forces within each individual conformation determines the energy of the state, and therefore the time it takes for it to unfold. Here we present a kinetic analysis of 2,625 unfolding events of poly-ubiquitin proteins using single-molecule force-clamp spectroscopy, with the aim of revealing the shape and breadth of the energy barrier distribution. A novel statistical analysis of the protein unfolding times opens the investigation of the energy fluctuations as a function of the stretching force, that is, the external perturbation, to experimentation. Mapping the statistical landscape features as a function of the external force provides a powerful new tool to precisely investigate the effects of non-equilibrium conditions on the conformational diversity of proteins.

In atomic force microscopy (AFM) experiments, the force-clamp technique provides ideal experimental conditions for the measurement of the kinetics of protein unfolding at a well-defined force¹⁸. We use a twelve-module ubiquitin protein construct in all of the experiments. However, the polyprotein molecules are picked up by the cantilever at random points on the surface, implying that any number of protein modules, $N \leq 12$, may be exposed to a force in a pulling experiment. The polyprotein is stretched at a calibrated constant force of 110 pN, causing the individual modules to unfold stochastically, as illustrated in Fig. 1a. Each unfolding event is accompanied by a release in length of 20 ± 0.9 nm, corresponding to the unravelling of a single ubiquitin module. Each length trajectory

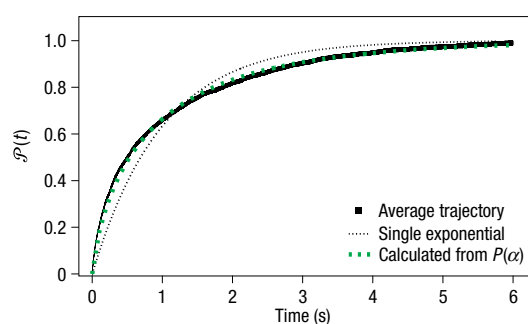


Figure 2 Average unfolding trajectory obtained by summing over 416 single-chain trajectories or 2,625 events (black curve), analogous to ensemble measurements. A single exponential fit serves as a test for the two-state model, with $\chi^2 = 40$ (black dashed curve). The average trajectory of all the data is compared with the weighted average predicted from the power-law distribution of rates, $P(\alpha)$, obtained experimentally in Fig. 4 (green dashed curve), with a much-improved agreement with the data.

over time therefore resembles a staircase, with each step marking the dwell time, t_k , of the k th module in a chain of N modules, as shown in Fig. 1b. We have collected 416 such unfolding trajectories, as shown in Fig. 1c, each containing between 3 and 12 unfolding steps, giving a total of 2,625 unfolding events. A minimum of three consecutive 20-nm steps in the staircase is required as the signature of the poly-ubiquitin molecule to be included in the analysis.

The two-state model of unfolding implies a stochastic (markovian) process with a single rate constant, which can be obtained from the single exponential fit to the average unfolding trajectory. Previously we have shown that the rate of unfolding, obtained from the average of just a few trajectories, is exponentially dependent on the force, and that the process at a constant force appears two-state¹⁸. With a much-improved statistical pool of 2,625 unfolding events at a constant force of 110 pN, summing over all the trajectories gives rise to the average trajectory that effectively counts the number of unfolding events as a function of time, as each unfolding event is marked by a 20-nm step in length. Normalizing by the total number of unfolding events and the protein length, we obtain the unfolding probability as a function of time, $\mathcal{P}(t)$, for all of the data, shown in Fig. 2. The fit is clearly distinct from a single exponential ($\chi^2 = 40$). The deviations from the fit may be indicative of alternative unfolding barriers in this ensemble measurement. The average rate constant, $\langle \alpha \rangle = 1.0 \text{ s}^{-1}$, is nevertheless in good agreement with previous results. The unfolding probability is independent of the number of modules in the chain, N , as we show in the Supplementary Information.

The challenge is then to decipher how diverse the rates of unfolding are within the system ensemble, assuming a non-homogeneous markovian process¹⁹. Therefore, we use the information at the single-molecule level to obtain the probability distribution, $P(\alpha)$, for the ensemble of single-molecule data. We approximate a rate constant, α , for the unfolding trajectory of each ubiquitin chain. Analogous to radioactive decay and the release of neurotransmitters in synaptic transmission²⁰, the probability of a single module unfolding in time t is assumed to be $(1 - e^{-\alpha t})$. This assumption is supported by the observation that each unfolding event takes place in a single-length step on the timescale of the experiment, as seen in Fig. 1b,c. The probability distribution of observing a sequence of unfolding modules in a single trajectory depends on N according to a binomial distribution. However, the unfolding trajectory of a polyprotein does not reveal N with

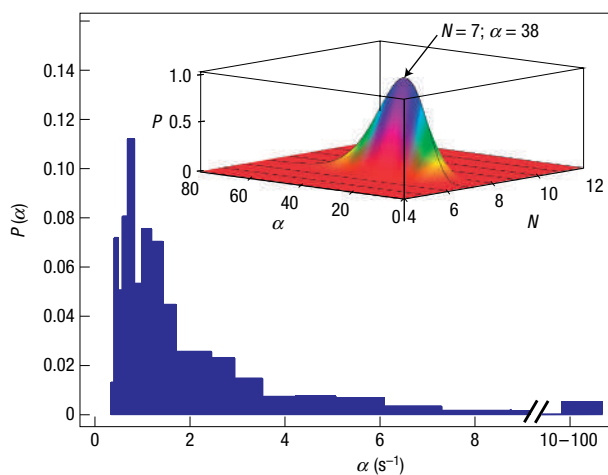


Figure 3 Normalized histogram of the unfolding rates of each poly-ubiquitin chain. From the sequence of dwell times to the unfolding events in every chain, we obtained the most likely rate α by maximizing the probability distribution in equation (1) as a function of α and N (between k_{\max} and 12). As the histogram does not capture the fast unfolding traces with $\alpha > 10 \text{ s}^{-1}$, the remainder of the data are represented in the last bar of the histogram. Inset: The probability map is shown for a single chain, with maximum P corresponding to $\alpha = 38 \text{ s}^{-1}$, $N = 7$.

certainty, because the molecule can detach from the cantilever before all of the modules unfold. The range of possible N is small, as it must lie between the number of observed steps, k_{\max} , and twelve, the length of the whole protein chain. For a given α , from the experimental data of a sequence of k events unfolding at the dwell times t_k , we have

$$P(t_1, \dots, t_k) = \alpha^{k_{\max}} N(N-1) \dots (N-k_{\max}+1) \times \exp\left(-\alpha \sum_{k=1}^{k_{\max}-1} t_k\right) e^{-\alpha(N-k_{\max}+1)t_{k_{\max}}}. \quad (1)$$

This is the product of probability distributions that ‘ k out of N ’ modules remain folded during each time interval between unfolding events in a single chain. For instance, for a chain with two unfolding events (green trace in Fig. 1c) whose first module unfolded at time t_1 and the second at time t_2 , equation (1) reduces to

$$P(t_1, t_2) = \alpha^2 N(N-1) e^{-\alpha t_1} e^{-\alpha(N-1)t_2}.$$

A probability map is calculated for each individual unfolding trajectory. We apply equation (1) to calculate the probability of a given sequence of unfolding times, t_k , occurring for all possible values of N , ranging from k_{\max} to 12, and α . The resulting probability map, shown in the inset of Fig. 3, shows that the most likely N and α are identified as the peak in the probability map. This is known as the maximum-likelihood method²¹, and is described in more detail in the Supplementary Information. The maxima of the probability maps for each trace give rise to a distribution $P(\alpha)$ for the whole set of data, shown in Fig. 3. As this histogram is plotted on a linear scale, it is difficult to capture the long tail of the distribution. Logarithmic binning of the data shown on a log-log plot reveals an unanticipated degree of complexity, shown in blue in Fig. 4. Although the unfolding process has a statistically preferred pathway, indicated as the peak $\alpha = 0.7 \text{ s}^{-1}$, we find a

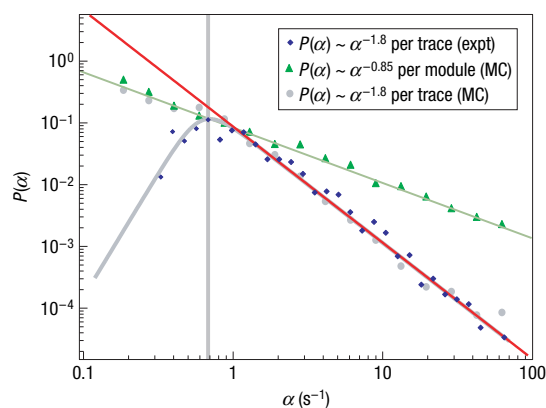


Figure 4 Histogram in Fig. 3 plotted on a log-log scale reveals a power-law distribution of rate constants (blue diamonds) per ubiquitin chain that spans more than two decades with a decay exponent $\gamma = 1.8$. Because the molecules detach from the cantilever at random times, the slow unfolding rates are under-represented in the distribution, giving rise to the peak. Furthermore, the maximum-likelihood method averages over unfolding events within each chain, which narrows the distribution. Monte Carlo (MC) simulations showed that the distribution of rates for each module within the chain (green triangles), with $\gamma = 0.85 \pm 0.05$, reproduces the experimental power-law tail of the distribution per trace (grey circles).

surprisingly broad distribution of rate constants, which follows a power law (red line),

$$P(\alpha) \propto \alpha^{-\gamma}.$$

The decay exponent, $\gamma = 1.8$, implies that the distribution does not have a well-defined average. The few data points defining the peak at very slow unfolding rates correspond to long-lasting experiments with a smaller statistical pool of data, which may be skewing the distribution up to $\alpha = 0.4 \text{ s}^{-1}$. The following discussion therefore only concerns the power-law tail of the distribution.

The existing power law spreads over two decades (without the peak), which we cannot extend due to experimental limitations. To monitor the non-equilibrium unfolding behaviour of a protein, we apply an external stretching force, which uses an electronic feedback system, limiting our time resolution to 10 ms. The fastest measurable rate constant is therefore 100 s^{-1} . On the slow end of the spectrum, the random detachment of the molecules from the cantilever and the presence of cantilever drift conspire against the measurement of long traces beyond 10 s. We are therefore limited to the measurement of rates of 0.1 s^{-1} . Even so, the distribution shows large deviations from the currently accepted two-state unfolding kinetics.

Owing to the averaging over each single-molecule chain of unfolding events, implicit to our maximum-likelihood method, it is expected that the same distribution for a monomeric protein is even broader, with $\gamma < 1.8$. Indeed, we quantified the effect of averaging by generating individual protein modules in each chain with power-law distributed rates of unfolding using Monte Carlo simulations. Then, we allocated the most likely rates to each single-molecule chain, as in the experiment. In Fig. 4, we show that the module-generated distribution of $P(\alpha) \propto \alpha^{-0.85 \pm 0.05}$ (green triangles) best reproduces the experimentally observed power-law distribution of rates per chain (grey circles). Further confidence in the validity of this result is obtained from the excellent fit of the average unfolding trajectory calculated assuming the experimental $P(\alpha)$

(blue diamonds) to the average trajectory of the raw experimental data, shown in Fig. 2 (green dashed trace), where maximum likelihood plays no role. The observed distribution in Fig. 4 is independent of the number of modules in the chain N , as $P(\alpha)$ with the same decay coefficient of $\gamma = 1.8$ is obtained by pooling data with different chain-length ranges, as shown in the Supplementary Information. This indicates that the individual modules are independent of one another, such that the length of the chain plays no role in the unfolding rate constant. Because the complex kinetics arises from the conformational heterogeneity on the level of the module, we interpret the results in terms of the modular distribution of unfolding rates.

How can we interpret a distribution of unfolding rate constants that spreads over two orders of magnitude under constant experimental conditions? This distribution could not be explained by the uncertainties associated with maximum likelihood²¹ nor the experimental noise in the force, given a single rate of unfolding in the system. The system's complex kinetics is then a consequence of the underlying roughness of the free-energy landscape^{1,22,23}. It could be argued that several discrete pathways between the folded and the unfolded state govern the broad distribution, as the data can be equally well fitted as a sum of at least three exponentials with different decay rates. However, such a large number of fitting parameters is highly degenerate, and so we postulate that it is much more likely that a continuous variation in α is giving rise to such a broad distribution.

The power-law-distributed rates can be deduced on physical grounds, by appealing to the notion that the energy of the folded protein can be represented as a multi-valley energy landscape². We assume that the only possibility for the protein to diffuse in the landscape is an energy-activated process to overcome the energetic barrier of height E , as implied by the Arrhenius law. This model is the simplest interpretation of our data. The applicability of the Arrhenius law to diffusion in glassy landscapes is much debated in the literature, and depends on whether the glass in question is classified as a 'strong' or a 'fragile' glass^{24,25}. Fragile glasses with very high energy barriers, such that activation is not possible, exhibit diffusion that is independent of the energy barriers in the system²⁶. On the other hand, the Arrhenius law assumes that the protein is a strong glass, in which the energy barriers are low enough to determine the activation process of unfolding.

Under this assumption, the time taken to escape from a given folded state and overcome a barrier of height E at temperature T is the inverse of the unfolding rate $\tau = 1/\alpha$ and can be described by

$$\tau = \tau_0 e^{E/k_B T}, \quad (2)$$

where τ_0 is a microscopic timescale and k_B is the Boltzmann constant. A simple change of variables converts the experimental $P(\alpha) \propto \alpha^{-0.85 \pm 0.05}$ per module into $P(\tau) \propto \tau^{-1.15 \pm 0.05}$, which can be conveniently represented as $\tau^{-(1+a)}$, where $a = 0.15 \pm 0.05$. The distribution of barriers, $P(E)$, therefore governs the distribution of trapping times, $P(\tau)$, through equation (2). Assuming the experimental distribution of $P(\tau)$, $P(E)$ is then expressed by an exponential distribution with average barrier height \bar{E}

$$P(E) = \frac{\tau_0^{-a}}{k_B T} e^{-E/\bar{E}},$$

with $\bar{E} = k_B T/a = 6.7 k_B T$, as shown in Fig. 5. The shaded region in the figure shows the experimental error in a , which implies that the average barrier height lies in the range between 5 and $10 k_B T$. The breadth of the energy-barrier distribution indicates high amplitude fluctuations in the landscape, much higher than thermally activated transitions. Systems in such landscapes have little preference for the

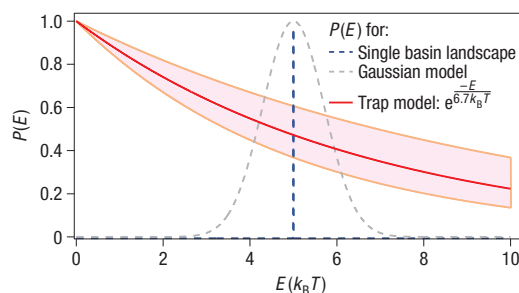


Figure 5 Shape and breadth of the distribution of energy barriers in the protein energy landscape under a constant force. The experimental data predicts the exponential distribution, according to the trap model (red curve). The highlighted area represents the possible error introduced by the uncertainty in the data, ranging between 5 and $10 k_B T$. Alternative energy landscapes, with gaussian fluctuations (grey dashed curve) or a two-state model (blue dashed line) are also shown.

ground native state, yet they fluctuate between structurally similar conformations. The exponential form of the energy distribution is typical of glasses, appearing in the random energy model²⁷ with applications in protein-folding simulations²⁸, as well as in experiments on glassy polystyrene²⁹.

The above results can be understood in the framework of the phenomenological 'trap' model of glasses³⁰, according to which the average energy characterizes the critical glass-transition temperature as $T_g = \bar{E}/k_B$ in proteins³¹. Below T_g the folded states exhibit frustration, and above it the landscape appears smooth with a single rate constant. Figure 5 schematically illustrates the different models of $P(E)$. In contrast to our findings, traditional two-state models would give rise to a single rate constant. Moreover, gaussian-distributed energies that do capture the roughness in funnel models^{7,32} would result in log-gaussian kinetics, which do not reproduce our experimental power-law distribution of unfolding times.

It has already been established how the force, F , influences the height of the average unfolding energy barrier, \bar{E} , along the ubiquitin-length reaction coordinate¹⁸. The energy-barrier height to unfolding, \bar{E}_a , is reduced by the work done in stretching the protein to the transition state, then the resulting barrier height, $\bar{E} = \bar{E}_a - F\Delta x$, where Δx is the distance to the transition state for unfolding. Provided that the transition state has roughly the same end-to-end length at all forces (0.14 nm), a larger force has been shown to reduce the barrier heights, on average, shifting the mean to a faster unfolding rate constant. However, the effect of force on the distribution of available conformations, and therefore energies, will depend on how the force distributes through the protein, microscopically, along the observed reaction coordinate. The answer to this question would require a three-dimensional investigation of stress transmission through the structure of the protein, testing the change in the configurational diversity of the protein in response to the applied force.

It is reasonable to assume that when the energy scale \bar{E} of the unfolding barriers becomes comparable to $k_B T$ at sufficiently high forces, the folded conformations will self-average, giving rise to two-state kinetics on a smooth energy landscape. Alternatively, raising the temperature above the measured T_g at 110 pN should induce two-state kinetics, although operating at such a high temperature would not be possible. Our result therefore indicates that ubiquitin under physiological conditions is inherently glassy, such that the proteins are 'frozen' in a given distribution of conformations.

Relating the power-law distribution of rates to protein conformational changes is an important task. Recent work, relating structure and dynamics of human ubiquitin (used in this study) fluctuating in solution⁹, shows structural motion of the order of 2 Å for individual amino acids. Mechanical stability of proteins has been shown to arise mainly from the backbone hydrogen-bonding pattern of the protein^{16,17}. We speculate that thermally driven rupture and formation of the hydrogen bonds causes fluctuations in the mechanical stability of the protein. These fluctuations are not reflected in our measured reaction coordinate of the end-to-end length, yet they manifest themselves through the broad distribution of $P(\alpha)$ that we observe. The connectivity of the states as a function of length is therefore still unclear, as there may be other coordinates through which they are locally connected in the multi-dimensional space. Molecular dynamics simulations have shown that the connections in the network of the conformational space of a folding protein are scale-free and have a native-state basin with a hierarchical organization of free energies³³, which may account for our observations. Their scale-free distribution is reminiscent of many diverse complex networks in biology³⁴, such as the protein structural network, protein-protein interaction network and the network of metabolic pathways, which have been shown to exhibit a fractal architecture, evolved according to a self-organizing principle in nature³⁵. Could the energy landscape of proteins be yet another example? This raises important questions about the relationship between the topology of the network and protein function. Although most protein engineering has so far been done on the basis of simple two-state models using ϕ value analysis¹⁵, it is becoming clear that point mutations may affect the distribution of states in more-complex ways, moderating the power-law decay coefficient or eliminating certain kinetic barriers in the landscape. Our results call for new methods of assessing the complex protein landscape, which are now amenable to experimentation using the techniques described in this paper.

METHODS

PROTEIN ENGINEERING

The polyprotein used in this study was a multiple-domain ubiquitin construct comprising twelve identical repeat units. The tandem repeats were formed by consecutive subcloning of the ubiquitin monomer using the 'sticky' ends of the BamHI and BglII restriction sites. The monomer was cloned from the native nine-unit ubiquitin by the polymerase chain reaction and isolated by agarose gel purification. The twelve-domain ubiquitin was cloned into the PQE16 (Qiagen) expression vector, and transformed into the BLR(DE3) *Escherichia coli* expression strain. This construct has a C-terminus His-tag and has two additional residues (arginine and serine) between each module in the chain. Constructs were expressed in BLR (DE3) *E. coli*, and purified by histidine metal-affinity chromatography with Talon resin (Clontech) and by gel-filtration using a Superdex 200 HR column (GE Biosciences).

SINGLE-MOLECULE AFM

We used a custom-made AFM under force-clamp conditions¹⁸. The sample was prepared by depositing 3–10 μ l protein in 50 μ l PBS, at a concentration of 10–100 μ g ml⁻¹, onto a freshly evaporated gold coverslip to allow the protein to adsorb onto the gold. Each cantilever (Si₃N₄, Digital Instruments) was calibrated in solution before the measurements. The spring constant was typically found to be 15 pN nm⁻¹. The cantilever was repeatedly placed in contact with the surface, exerting a significant force of several hundred piconewtons, causing the polyprotein molecules to adhere non-specifically to the cantilever tip. The piezo was then retracted to produce a set constant force, while the extension was recorded. An active feedback mechanism was used to maintain the constant force for ten seconds. As the molecules detach from the

cantilever at random times, we only include trajectories with a detachment time of at least 2.5 s to minimize the error in the maximum-likelihood method. All experiments were carried out at room temperature.

Received 12 December 2005; accepted 3 February 2006; published 1 April 2006.

References

1. Ansari, A. *et al.* Protein states and proteinquakes. *Proc. Natl Acad. Sci. USA* **82**, 5000–5004 (1985).
2. Frauenfelder, H., Sligar, S. G. & Wolynes, P. The energy landscapes and motions of proteins. *Science* **254**, 1598–1603 (1991).
3. Karplus, M., Gao, Y. Q., Ma, J., van der Vaart, A. & Yang, W. Protein structural transitions and their functional role. *Phil. Trans. A* **363**, 331–356 (2005).
4. Bryngelson, J. D., Onuchic, J. N., Socci, N. D. & Wolynes, P. G. Funnel, pathways, and the energy landscape of protein folding: a synthesis. *Proteins* **21**, 167195 (1995).
5. Dill, K. A. *et al.* Principles of protein folding — a perspective from simple exact models. *Protein Sci.* **4**, 561–602 (1995).
6. Lazaridis, T. & Karplus, M. 'New view' of protein folding reconciled with the old through multiple unfolding simulations. *Science* **278**, 1928–1931 (1997).
7. Hyeon, C. & Thirumalai, D. Can energy landscape roughness of proteins and RNA be measured by using mechanical unfolding experiments? *Proc. Natl Acad. Sci. USA* **100**, 10249–10253 (2003).
8. Kneller, G. R. Quasielastic neutron scattering and relaxation processes in proteins: analytical and simulation-based models. *Phys. Chem. Chem. Phys.* **7**, 2641–2655 (2005).
9. Lindorff-Larsen, K., Best, R. B., DePristo, M. A., Dobson, C. M. & Vendruscolo, M. Simultaneous determination of protein structure and dynamics. *Nature* **433**, 128–132 (2005).
10. Xue, Q. & Yeung, E. S. Differences in the chemical reactivity of individual molecules of an enzyme. *Nature* **373**, 681–683 (1995).
11. van Oijen, A. M. *et al.* Single-molecule kinetics of lambda exonuclease reveal base dependence and dynamic disorder. *Science* **301**, 1235–1238 (2003).
12. Itoh, K. & Sasaki, M. Dynamical transition and proteinquake in photoactive yellow protein. *Proc. Natl Acad. Sci. USA* **101**, 14736–14741 (2004).
13. Yang, H. *et al.* Protein conformational dynamics probed by single-molecule electron transfer. *Science* **302**, 262–266 (2003).
14. Min, W., Luo, G., Cherayil, B. J., Kou, S. C. & Xie, X. S. Observation of a power-law memory kernel for fluctuations within a single protein molecule. *Phys. Rev. Lett.* **94**, 198302 (2005).
15. Fersht, A. R. *Structure and Mechanism in Protein Science* (Freeman, New York, 1992).
16. Carrion-Vazquez, M. *et al.* Protein nanomechanics — as studied by single-molecule force spectroscopy AFM. *Biophys. J.* **75**, 662–671 (1998).
17. Li, H. B., Carrion-Vazquez, M., Oberhauser, A. F., Marszalek, P. E. & Fernandez, J. M. Point mutations alter the mechanical stability of immunoglobulin modules. *Nature Struct. Biol.* **7**, 1117–1120 (2000).
18. Schlierf, M., Li, H. & Fernandez, J. M. The unfolding kinetics of ubiquitin captured with single-molecule force-clamp techniques. *Proc. Natl Acad. Sci. USA* **101**, 7299–7304 (2004).
19. Ross, S. *Stochastic Processes* (Wiley, New York, 1996).
20. Johnston, D. & Wu, S. M. *Foundations of Cellular Neurophysiology* (MIT Press, Cambridge, Massachusetts, 1995).
21. Colquhoun, D., Hattton, C. J. & Hawkes, A. G. The quality of maximum likelihood estimates of ion channel rate constants. *J. Physiol.* **547**, 699–728 (2003).
22. Chekmarev, S. F., Krivov, S. V. & Karplus, M. Folding time distributions as an approach to protein folding kinetics. *J. Phys. Chem. B* **109**, 5312–5330 (2005).
23. Lee, C., Stell, G. & Wang, J. First passage time distribution and non-markovian diffusion dynamics of protein folding. *J. Chem. Phys.* **118**, 959–968 (2003).
24. Angell, C. A. Perspective on the glass-transition. *J. Phys. Chem. Solids* **49**, 863–871 (1988).
25. Lubchenko, V. & Wolynes, P. G. Theory of aging in structural glasses. *J. Chem. Phys.* **121**, 2852–2865 (2004).
26. Marques, M. I. & Stanley, H. E. Relationship between fragility, diffusive directions and energy barriers in a supercooled liquid. *Physica A* **345**, 395–403 (2005).
27. Derrida, B. Random-energy model — limit of a family of disordered models. *Proc. Natl Acad. Sci. USA* **45**, 79–82 (1980).
28. Pande, V., Grosberg, A. & Tanaka, T. Statistical mechanics of simple models of protein folding and design. *Biophys. J.* **73**, 3192–3210 (1997).
29. Bercu, V., Martinelli, M., Massa, C., Pardi, L. & Leporini, D. A study of the deep structure of the energy landscape of glassy polystyrene: the exponential distribution of the energy barriers revealed by high-field electron spin resonance spectroscopy. *Biophys. J.* **16**, L479–L488 (2004).
30. Monthus, C. & Bouchaud, J. Models of traps and glass phenomenology. *J. Phys. A* **29**, 3847–3869 (1996).
31. Lee, A. L. & Wand, A. J. Microscopic origins of entropy, heat capacity and the glass transition in proteins. *Nature* **411**, 501–504 (2004).
32. Nevo, R., Brumfeld, V., Kapon, R., Hinterdorfer, P. & Reich, Z. Direct measurement of protein energy landscape roughness. *EMBO Rep.* **6**, 482–486 (2005).
33. Rao, F. & Cafilisch, A. The protein folding network. *J. Mol. Biol.* **342**, 299–306 (2004).
34. Barabási, A.-L. & Oltvai, Z. N. Network biology: understanding the cell's functional organization. *Nature* **5**, 101–113 (2004).
35. Song, C., Havlin, S. & Makse, H. A. Self-similarity of complex networks. *Nature* **433**, 392–395 (2005).

Acknowledgements

We would like to thank H. H. Huang for making the ubiquitin construct, S. Garcia-Manyes for data collection, and H. A. Makse and A. J. Tolley for enlightening discussions. This work has been supported by NIH grant R01 HL66030 to J.M.F. Correspondence and requests for materials should be addressed to J.B. or J.M.F. Supplementary Information accompanies this paper on www.nature.com/naturephysics.

Competing financial interests

The authors declare that they have no competing financial interests.

Reprints and permission information is available online at <http://npg.nature.com/reprintsandpermissions/>